Supporting Information

Highly stable and efficient cathode-buffer-layer-free inverted perovskite solar cells

Yong Ryun Kim[a], Chang Mok Oh[b], Chang Jae Yoon[a], Ju-Hyeon Kim[c], Kiyoung Park[c], Kwanghee Lee[a,c*], In-Wook Hwang[b*], Heejoo Kim[d*]

[a]*Research Institute for Solar and Sustainable Energies (RISE), Gwangju Institute of Science and Technology (GIST), Gwangju 61005, Republic of Korea*

[b]*Advanced Photonics Research Institute (APRI), Gwangju Institute of Science and Technology, Gwangju 61005, Republic of Korea*

[c]*Heeger Center for Advanced Materials (HCAM), Gwangju Institute of Science and Technology (GIST), Gwangju 61005, Republic of Korea*

[d]*Graduate School of Energy Convergence, Institute of Integrated Technology, Gwangju Institute of Science and Technology (GIST), Gwangju 61005, Republic of Korea*

Corresponding Author

* E-mail: klee@gist.ac.kr (Kwanghee Lee), hwangiw@gist.ac.kr (In-wook Hwang), Heejook@gist.ac.kr (Heejoo Kim),

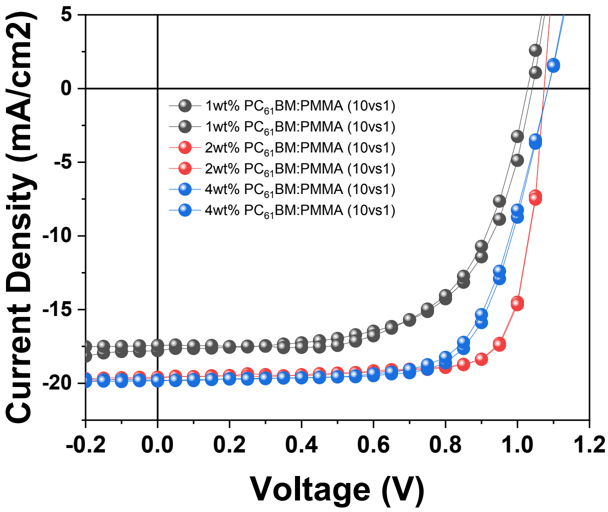

Fig S1. – The *J-V* of the I-PeSCs fabricated using various wt.% $PC_{61}BM$ dispersed in 1wt% of PMMA (the volume ratio 10 vs 1); Device structures of ITO/PTAA/PFN-Br/$MAPbI_3$/$PC_{61}BM$:PMMA/Cu were used

Table S1. – Photovoltaic device parameters for I-PeSCs fabricated using the device structures of ITO/PTAA/PFN-Br/$MAPbI_3$/$PC_{61}BM$/Cu and ITO/PTAA/PFN-Br/$MAPbI_3$/$PC_{61}BM$:PMMA/Cu

ETLs	Spin-coating speed (rpm)	Sweep Direction	V_{oc} (V)	J_{sc} (mA/cm^2)	FF	PCE (%)
$PC_{61}BM$ (1wt%):PMMA (1wt%)	2000	Forward	1.04	17.78	0.62	11.42
		Reverse	1.03	17.42	0.63	11.24
$PC_{61}BM$ (2wt%):PMMA (1wt%)	2000	Forward	1.07	19.67	0.78	16.53
		Reverse	1.07	19.59	0.79	16.55
$PC_{61}BM$ (4wt%):PMMA (1wt%)	2000	Forward	1.06	19.86	0.72	15.19
		Reverse	1.06	19.88	0.74	15.61

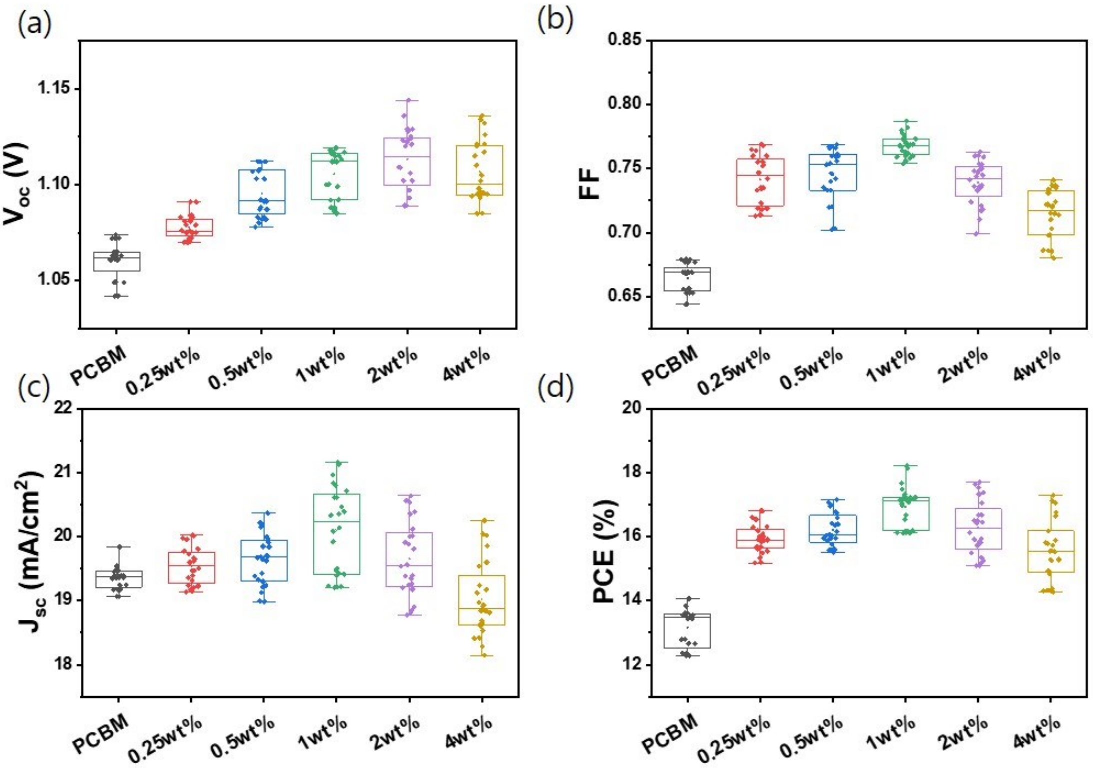

Fig S2. – Statistical distribution of the device parameters for I-PeSCs fabricated using various wt.% PMMA in $PC_{61}BM$; (a) V_{oc}, (b) FF, (c) J_{sc}, and (d) PCE. Device structures of ITO/PTAA/PFN-Br/$MAPbI_3$/$PC_{61}BM$ and ITO/PTAA/PFN-Br/$MAPbI_3$/$PC_{61}BM$:PMMA/Cu were used

Table S2. – Photovoltaic device parameters for I-PeSCs fabricated using the device structures of ITO/PTAA/PFN-Br/$MAPbI_3$/$PC_{61}BM$/Cu and ITO/PTAA/PFN-Br/$MAPbI_3$/$PC_{61}BM$:

PMMA/Cu

PMMA (wt%)	***V_{oc}* (V)**	***J_{sc}* (mA/cm^2)**	**FF**	**PCE (%)**
$PC_{61}BM$	1.068±0.011	19.37±0.19	0.66±0.01	13.15±0.56
0.25	1.077±0.006	19.45±0.36	0.72±0.02	15.74±0.59
0.5	1.094±0.012	19.47±0.49	0.74±0.02	16.05±0.58
1.0	1.104±0.012	19.94±0.71	0.76±0.01	16.72±0.728
2.0	1.113±0.015	18.78±0.69	0.74±0.02	16.02±0.94
4.0	1.106±0.015	18.94±0.60	0.71±0.02	15.30±1.06

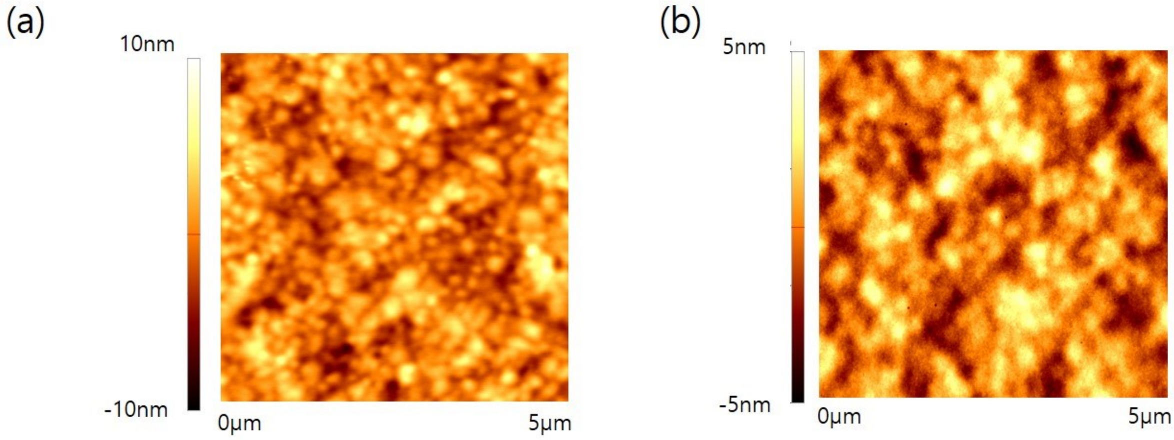

Fig S3. – AFM topographic images obtained from the PMMA sides of (a) ITO/PTAA/PFN-Br/$MAPbI_3$/PMMA(2 wt.%) and (b) ITO/PTAA/PFN-Br/$MAPbI_3$/PMMA(4 wt.%) films.

Table S3. – Photovoltaic device parameters for I-PeSCs fabricated using device structures of ITO/PTAA/PFN-Br/$MAPbI_3$/$PC_{61}BM$/Cu, ITO/PTAA/PFN-Br/$MAPbI_3$/$PC_{61}BM$/BCP/Cu, and ITO/PTAA/PFN-Br/$MAPbI_3$/$PC_{61}BM$:PMMA/Cu

ETL	Electrode	Sweep Direction	V_{oc} (V)	J_{sc} (mA/cm^2)	FF	PCE (%)	IPCE
$PC_{61}BM$	Cu	Forward	1.06	19.34	0.66	13.49 (13.08)	18.7
		Reverse	1.07	19.39	0.66	13.55 (13.20)	
$PC_{61}BM$/BCP	Cu	Forward	1.09	21.25	0.77	17.80 (17.64)	21.02
		Reverse	1.09	21.12	0.77	17.88 (17.64)	
$PC_{61}BM$:PMMA	Cu	Forward	1.12	20.83	0.78	18.21 (17.73)	21.07
		Reverse	1.12	20.80	0.79	18.38 (18.00)	

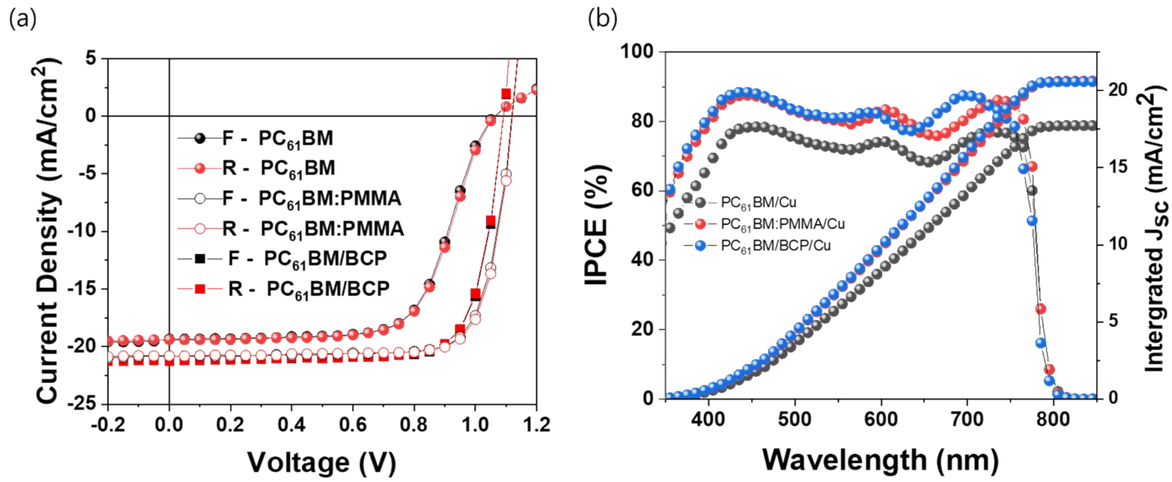

Fig S4. – (a) *J-V* and (b) IPCE plots for the best performance I-PeSCs fabricated using $PC_{61}BM$, $PC_{61}BM$/BCP, and $PC_{61}BM$:PMMA as ETLs

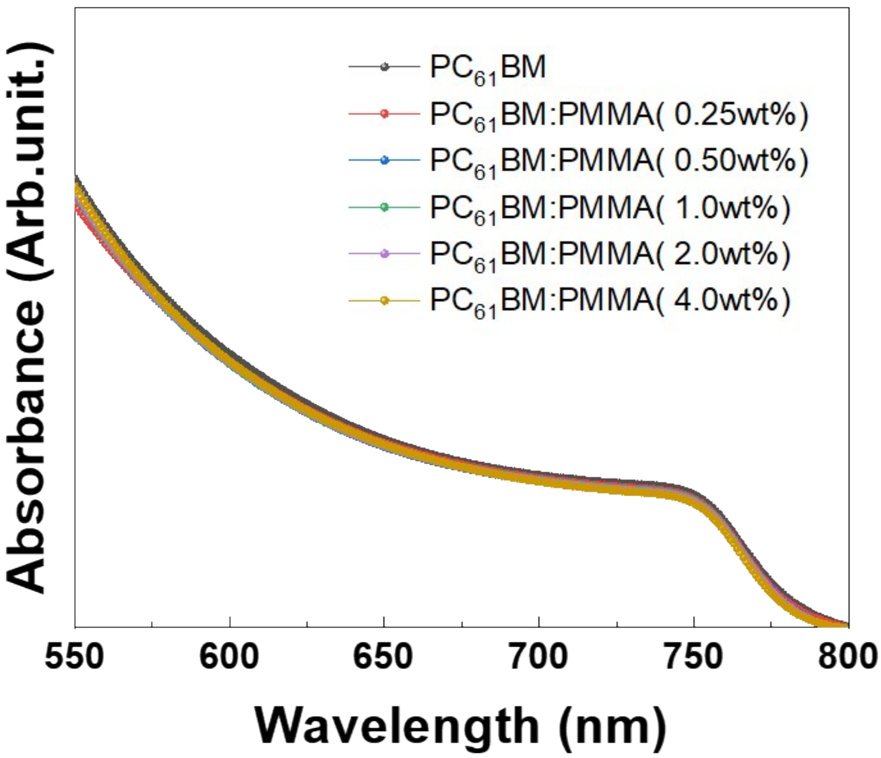

Fig S5. – UV-vis absorption spectra for films of ITO/PTAA/PFN-Br/$MAPbI_3$/$PC_{61}BM$ and ITO/PTAA/PFN-Br/$MAPbI_3$/$PC_{61}BM$:PMMA fabricated using various concentrations of PMMA in $PC_{61}BM$

Table S4. - Energy levels obtained from ultraviolet photoelectron spectra (UPS) for Cu electrode with $PC_{61}BM$ and $PC_{61}BM$:PMMA

Sample	$E_{cut-off}$ (eV)	IE- (hv – $E_{cut-off}$)	E_v(eV)	hv – $E_{cut-off}$ (eV)
Cu/$PC_{61}BM$	16.22	0.79	5.77	4.98
Cu/$PC_{61}BM$:PMMA	17.08	1.92	6.04	4.12

Table S5. – Parameters obtained from measurement of impedances in I-PeSCs fabricated using $PC_{61}BM$ and $PC_{61}BM$:PMMA as ETLs

ETL	R_p (Ω)	R_s (Ω)	CPE.
$PC_{61}BM$	273.43	26.93	0.801
$PC_{61}BM$:PMMA	44.10	24.21	0.914

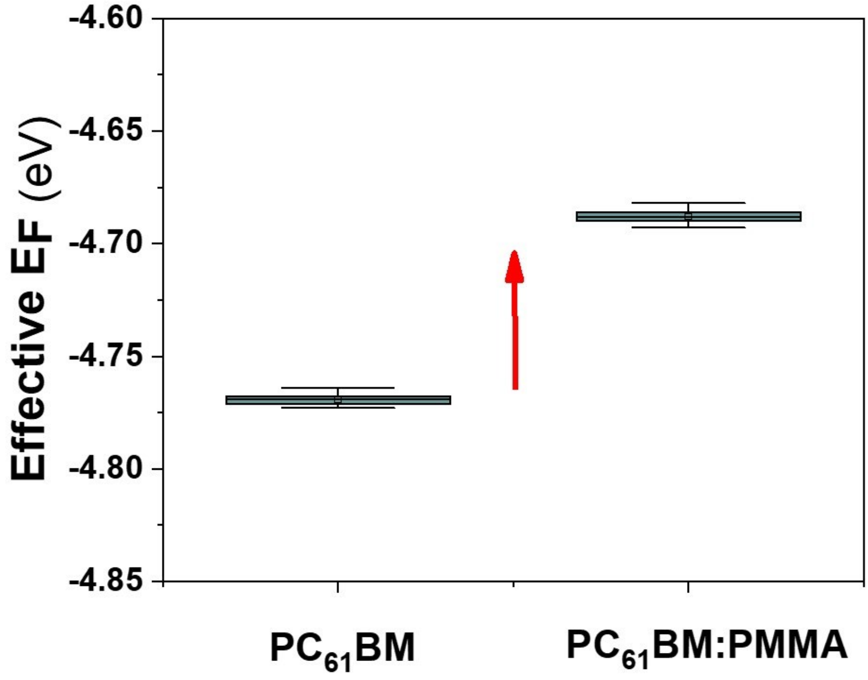

Fig S6. – Energy levels characterized by measurement of Kelvin probe for films of ITO/$PC_{61}BM$ and ITO/$PC_{61}BM$:PMMA

Table S6. – Trap density ($N_{trap-density}$) and mobility (α) calculated from the data plots for electron-only devices fabricated using the structures of $C_{60}/MAPbI_3/PC_{61}BM/Cu$ and $C_{60}/MAPbI_3/PC_{61}BM:PMMA/Cu$. The trap-filled-limit voltages (V_{TFL}) for the electron-only devices fabricated using PCBM and $PC_{61}BM$:PMMA as ETLs are 1.025 eV and 0.8 eV, respectively. The entire trap density ($N_{trap-density}$) in the $MAPbI_3$ layers is calculated by using the equation $N_{trap-density} = \frac{2\varepsilon_r\varepsilon_0 V_{TFL}}{ed^2}$, where ε_r is the dielectric constant of $MAPbI_3$, ε_0 is the vacuum permittivity (8.85 × 10^{-14} Fcm^{-1}), e is the charge constant (1.69 × 10^{-19} C), and d is the thickness of the $MAPbI_3$ layer, respectively

ETL	$N_{Trap\ Density}$ (cm^{-3})	α ($cm^2V^{-1}s^{-1}$)
	Electron	
$PC_{61}BM$	5.41×10^{15}	7.75×10^{-2}
$PC_{61}BM$:PMMA	3.54×10^{15}	7.86×10^{-2}

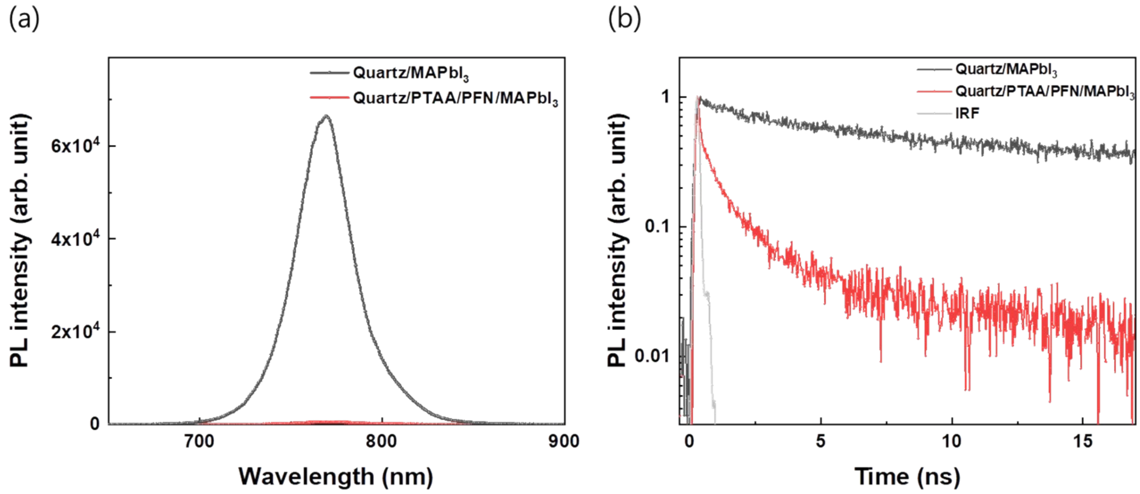

Fig S7. (a) Steady-state PL spectra and (b) TRPL decays of films of quartz/$MAPbI_3$ and quartz/PTAA/PFN-Br/$MAPbI_3$. The PL intensity of the perovskite was quenched by 99.5% in the quartz/PTAA/PFN-Br/$MAPbI_3$ film. In the TRPL, an excitation and detection wavelength of 470 nm and 770 nm was used. IRF represents instrument response function of the TCSPC system. The PL and TRPL data were obtained by photoexciting the quartz side of the films for observing the hole transfer process at the perovskite and HTL interface. Based on fitting the data with the use of bi-exponential functions, we obtained decay-time constants of 0.3 ns (99 %) and 1.3 ns (1 %) in the quartz/PTAA/PFN-Br/$MAPbI_3$ film

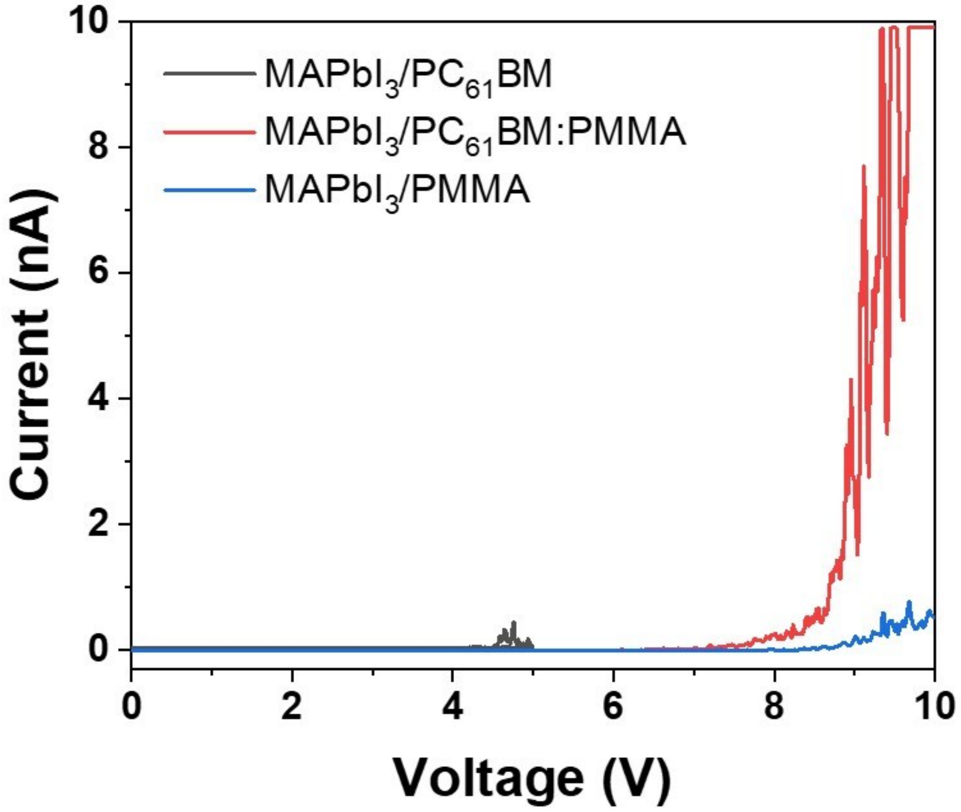

Fig S8. - Mean IV profiles extracted from several points of AFM topographic images in Fig. S2 (c) to (e)

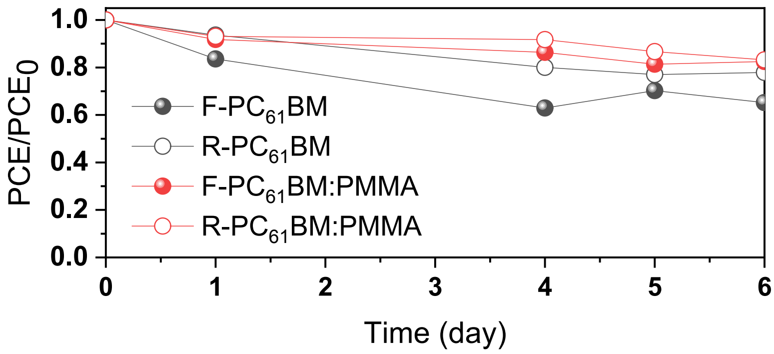

Fig S9. - Stability measurement for I-PeSCs plotted as a function of storage time under ambient air at 25 °C with a relative humidity of 20~45% for the active area of 1 cm^2